Dynamics of visons and thermal Hall effect in perturbed Kitaev models

Aprem P. Joy and Achim Rosch
Institute for Theoretical Physics, University of Cologne, Cologne, Germany
(Dated: September 2, 2021)

A vison is an excitation of the Kitaev spin liquid which carries a $\mathbb{Z}_2$ gauge flux. While immobile in the pure Kitaev model, it becomes a dynamical degree of freedom in the presence of perturbations. We study an isolated vison in the isotropic Kitaev model perturbed by a small external magnetic field h, an offdiagonal exchange interactions Γ and a Heisenberg coupling J. In the ferromagnetic Kitaev model, the dressed vison obtains a dispersion linear in Γ and h and a fully universal low-T mobility, $\mu = 6v_m^2/T^2$, where v_m is the velocity of Majorana fermions. In contrast, in the antiferromagnetic Kitaev model interference effects preclude coherent propagation and an incoherent Majorana-assisted hopping leads to a T-independent mobility. The motion of a single vison due to Heisenberg interactions is strongly suppressed for both signs of the Kitaev coupling. Vison bands induced by h are topological and lead to a characteristic peak in the thermal Hall effect as observed experimentally in α-$RuCl_3$.

Gauge theories are central to our understanding of high-energy physics where they mediate interactions between fundamental particles. While in the standard model the existence of gauge symmetries is postulated, they 'emerge' naturally in the description of certain strongly correlated solid-state systems. Such systems host fractional excitations with exotic quantum numbers. In this context, one of the best understood models is the honeycomb Kitaev model which hosts a spin liquid in its ground state [1]. In this two-dimensional model the magnetic spin fractionalizes into Majorana fermions coupled to a static $\mathbb{Z}_2$ gauge field. This allows to map the problem to that of non-interacting Majorana fermions making it an exactly solvable model. In the Kitaev model, the primary excitation of the gauge field is the vison which carries half a flux quantum. Visons are ubiquitous in $\mathbb{Z}_2$ lattice gauge theories and have been predicted in several systems [2–4] but have eluded experimentalists to date. Besides their fundamental importance in predicting signatures of $\mathbb{Z}_2$ spin liquids, they are much sought after for topological quantum information processing [1, 5].

Within the Kitaev model, a vison is an immobile finite-energy excitation, strongly interacting with the gapless Majorana fermions via its flux. The vison should therefore be viewed as a kind of 'polaronic' excitation: a π flux dressed by a cloud of Majorana fermions. Adding perturbations to the Kitaev model will generically make the gauge field a dynamical degree of freedom with mobile visons.

Remarkably, there are a number of materials which are believed to be approximately described by the Kitaev model. The past decade witnessed a surge of experimental efforts to detect fractionalization in such *Kitaev materials* [6–10]. Arguably, the most direct evidence so far for an exotic spin liquid phase have been reports of an approximately half-integer [11–14] quantized thermal Hall effect in a magnetic field in α-$RuCl_3$ expected to occur in chiral spin liquids coupled to phonons [15, 16]. Direct experimental signatures of visons, or - more generally - of emergent dynamical gauge fields, are, however, still missing. From the theory side, new detection protocols exploiting vison-Majorana interactions in the pure Kitaev limit have been proposed in recent works. This include local probes like STM [17–20], interplay of disorder and fractionalization [21, 22], and spin transport [23].

In all real materials the presence of further spin interactions besides the Kitaev coupling [6, 10, 24, 25] is unavoidable. Such terms, if sufficiently strong, destroy the spin liquid phase, often inducing magnetic ordering. In this case the fractionalized quasiparticles cease to be the most natural description of the model. Several numerical and mean-field studies have investigated the phase diagram of the Kitaev model in the presence of other interactions [6, 26–31] and provided useful insights. One interesting feature is, for example, that the ferromagnetic Kitaev model turns out to be much more fragile towards perturbations by either an off-diagonal symmetric exchange (Γ term) [28, 29, 31] or a magnetic field [27, 30]. The zero temperature phase transitions triggered by vison-pair (located on two adjacent plaquettes) dynamics have been studied by Zhang and collaborators recently [32, 33]. In a $\mathbb{Z}_2$ gauge theory, such vison pairs do not carry a net flux. The question whether an isolated vison, which defines due to its fractional flux a singular perturbation for the gapless fermions, is a coherent particle with a well defined mass is a non-trivial question and is largely unexplored. In this paper we provide a controlled calculation of the dynamics of single visons in the limit where perturbations by non-Kitaev terms are weak.

Model – We consider the isotropic honeycomb Kitaev model [1] in the presence of small perturbations,

$$H = H_K + \Delta H_h + \Delta H_\Gamma + \Delta H_J \tag{1}$$

$$H_K = K \sum_{<ij>_\gamma} \sigma_i^\gamma \sigma_j^\gamma. \tag{2}$$

In the pure Kitaev model, H_K, each site on the honeycomb lattice connects to its three neighbors with different components $\gamma = x, y, z$ of the spin. We mainly focus on two types of perturbations, a magnetic field in the [111] direction and an off-diagonal symmetric interaction, the

so-called Γ term

$$\Delta H_h = -h \sum_{i,\alpha} \frac{(1,1,1)}{\sqrt{3}} \cdot \boldsymbol{\sigma}_i \tag{3}$$

$$\Delta H_\Gamma = \Gamma \sum_{\langle ij\rangle_\gamma;\alpha,\beta\neq\gamma} \left(\sigma_i^\alpha \sigma_j^\beta + \sigma_i^\alpha \sigma_j^\beta\right). \tag{4}$$

Furthermore, we will also comment on the effects of perturbations arising from an isotropic Heisenberg term $\Delta H_J = J \sum_{<ij>} \boldsymbol{\sigma}_i \cdot \boldsymbol{\sigma}_j$.

The pure Kitaev model can be solved exactly [1] by mapping each spin to four Majorana fermion operators b^x, b^y, b^z and c on each lattice site with $\sigma_i^\alpha = i b_i^\alpha c_i$. The Kitaev Hamiltonian becomes

$$H = -K \sum_{<ij>_\gamma} i \hat{u}_{ij}^\gamma c_i c_j, \tag{5}$$

where the "link operators" $\hat{u}_{ij} = i b_i^\alpha b_j^\alpha$ commute with the Hamiltonian, takes eigenvalues ± 1 and is identified with a $\mathbb{Z}_2$ gauge field. The honeycomb lattice splits into two sublattices, A and B, and in the following we will use a convention where $i \in A$ and $j \in B$. On each link we define *bond fermions* χ [34] and in each unit cell *matter fermions*

$$\chi_{\langle ij\rangle_\alpha} = b_i^\alpha + i b_j^\alpha, \qquad f_i = c_i + i c_j. \tag{6}$$

The gauge variable $\hat{u}_{\langle ij\rangle_\alpha} = 2\chi^\dagger_{\langle ij\rangle_\alpha}\chi_{\langle ij\rangle_\alpha} - 1$ now becomes the parity of the bond fermion.

This spin-Majorana mapping necessarily enlarges the Hilbert space of the original spin model. The projection operator $\hat{P}$ is used to project out unphysical states.

$$\hat{P} = \prod_k \frac{(1+\hat{D}_k)}{2}, \qquad \hat{D}_k = b_k^x b_k^y b_k^z c_k. \tag{7}$$

From the gauge theoretical perspective, $\hat{P}$ induces a summation over all $\mathbb{Z}_2$ gauge transformations.

Visons – The physical degree of freedom encoded in the $\mathbb{Z}_2$ gauge field is the flux of each hexagonal plaquette. The plaquette operator $\hat{W}_p = \prod_{\hexagon} \sigma_i^\gamma \sigma_j^\gamma = \prod_{\hexagon} u_{ij}$ with eigenvalues ± 1 commutes with H_K. In the ground state of H_K, $W_p = 1$ on all plaquettes describing a flux-free state. A vison is the gauge excitation with lowest energy obtained by setting one of the $\hat{W}_p = -1$, thus creating a π flux. In systems with periodic boundary conditions (PBC) visons can only be created in pairs but with open boundary conditions (OBC) a single vison is a well defined excitation [1] with a finite energy cost $E_0^v \approx 0.1535|K|$.

Within the gauge theory description, one can describe a vison by a string of flipped link variables $u_{ij} = -1$. This string extends to the boundary (OBC) or connects a pair of visons (PBC). To handle this unphysical gauge string while calculating gauge invariant quantities, we find it useful to project the wave functions back to the physical Hilbert space.

$$|\Phi(\boldsymbol{R})\rangle = \hat{P}\,|\mathcal{G}(\boldsymbol{R})\rangle\,|M(\mathcal{G})\rangle\,. \tag{8}$$

Here $\boldsymbol{R}$ denotes the position of the vison, $|\mathcal{G}(\boldsymbol{R})\rangle$ is the wavefunction describing the gauge sector (i.e., the bond fermions) while $|M(\mathcal{G})\rangle$ is the many-body wavefunction of the Majorana fermions in a fixed gauge $\mathcal{G}$. Importantly, $\hat{P}$ projects the wavefunction onto the physical Hilbert space.

To avoid numerical problems related to dangling bonds and spurious boundary modes, we do all of our calculations with periodic boundary conditions, placing two visons at maximal separation. Using exact diagonalization, we typically consider systems with linear dimensions up to 80 corresponding to 12.800 sites.

1st order PT: FM Kitaev – We now turn to the case with small perturbations $\Delta H = \Delta H_\Gamma, \Delta H_h$. These terms obviously break the exact solubility of the pure Kitaev model as the plaquette operators are no more conserved. Thus the gauge field becomes a dynamical degree of freedom, visons are created and destroyed by quantum and thermal fluctuations and they become mobile. Importantly, the vison number remains conserved modulo 2 and thus a single vison cannot decay but remains a stable quasiparticle. To linear order in the perturbations, the hopping rate of the vison can be computed from

$$t_{ab} = \langle \Phi_0(\boldsymbol{R}_a)|\,\Delta H\,|\Phi_0(\boldsymbol{R}_b)\rangle\,. \tag{9}$$

The second vison in our system is kept at a fixed position, while computing the hopping from vison position $\boldsymbol{R}_b$ to $\boldsymbol{R}_a$. The computation of this harmless-looking overlap, discussed in App. A, turns out to be non-trivial for three reasons. First, it is important to use the projection operator $\hat{P}$ in Eq. (7) to be able to match different gauges. Second, one has to calculate fermionic matrix elements involving the overlap of two different many-particle Majorana states and corresponding Bogoliubov vacua which can be done using methods developed by Robledo [35, 36]. Third, some (but not all) of the matrix elements have strong finite size effects probably related to the presence of a gapless spectrum and quasi-localized states induced by the vison [37, 38]. For the ferromagnetic Kitaev model, $K < 0$, the Γ term induces a next-nearest neighbor hopping t_Γ of the vison (on the dual triangular lattice formed by the plaquettes). Fig. 1a shows that finite size effects are almost absent and we obtain

$$t_\Gamma \approx -1.495\,\Gamma. \tag{10}$$

In Fig. 1c, the resulting band structure is shown. Within our approximation all bands are three-fold degenerate as the next-nearest neighbour hopping connects only states within one of three sublattices. For $\Gamma < 0$, the minima of the dispersion are located the Γ, K and K' points, while for $\Gamma > 0$ there are 6 minima located on the lines connecting the Γ and M points.

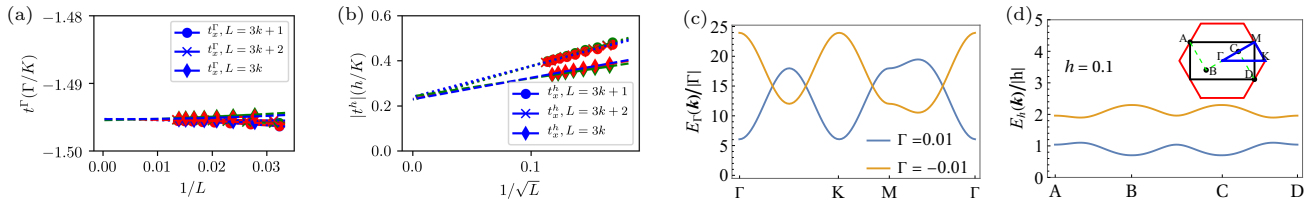

FIG. 1: Vison hopping amplitudes for $K = -1$ as function of inverse system size, $L = 3k+n$, $k \in \mathbb{N}$, $n = 0, 1, 2$ for a perturbation by a small Γ term (panel (a), next-nearest neighbor hopping) and a small magnetic field h (panel (b), imaginary-valued nearest neighbor hopping). Color code: green - t_y^ζ, red - t_z^ζ where $\zeta = h, \Gamma$. In panel (c) and (d) the corresponding vison dispersions are shown.

The magnetic field on the other hand, induces a nearest neighbour hopping with a purely imaginary hopping amplitude

$$t_h \approx \pm 0.22 i\, h. \tag{11}$$

This quantity, however, shows strong finite size effects, see Fig. 1b. The estimate Eq. (11) has been obtained from an extrapolation to $L \to \infty$ assuming that finite size effects scale with $\mathcal{O}(L^{-\frac{1}{2}})$, see Fig. 1b. This gives consistent values for system sizes $L = 3k + n$ for large $k \in \mathbb{N}$ and $n = 0, 1, 2$.

t_h is purely imaginary which simply follows from the fact that the magnetic field h is odd under time reversal. Thus the vison will pick up a phase $\pm i = e^{\pm i\pi/2}$ when hopping on a triangular loop. To determine the sign, we calculate $\arg\left[\langle \boldsymbol{R}_1|\Delta H_h|\boldsymbol{R}_3\rangle\langle \boldsymbol{R}_3|\Delta H_h|\boldsymbol{R}_2\rangle\langle \boldsymbol{R}_2|\Delta H_h|\boldsymbol{R}_1\rangle\right] = \mathrm{sign}(h)\frac{\pi}{2}$ for three vison sites ordered anticlockwise around a honeycomb site. Thus each triangular vison plaquette (i.e, each site of the original honeycomb lattice) carries a flux of $+\pi/2$ for $h > 0$ ($-\frac{\pi}{2}$ for $h < 0$). This sign is consistent with the algebraic relation $\sigma_z\sigma_y\sigma_x = -i$ and will become important when we calculate the thermal Hall effect due to visons below. The flux lattice leads to a doubling of the unit cell (containing two triangular plaquettes each) and results in two vison bands in a reduced Brillouin zone (see Fig. 1d), with non-trivial topology characterised by Chern numbers ± 1.

Mobility – So far we have shown that a dressed vison obtains a finite hopping amplitude linear in h and Γ at zero temperature. At finite temperatures, thermally excited gapless Majoranas will scatter from the vison, leading to friction and a finite mobility of the vison. The mobility μ describes the finite velocity v obtained by a vison in the presence of external forces, $\langle v\rangle = \mu F$. Via the Einstein relation $D = \mu k_B T$ the mobility is directly related to the diffusion constant of the vison which characterizes its dynamics. Note that calculation of the mobility of a vison is qualitatively different from the problem of the mobility of a vortex in a d-wave superconductor where extra complications arise due to the presence of Goldstone modes and the external magnetic field [39–41]. Here, we only consider the effect of the Γ perturbation for $K < 0$ to avoid technical complications related to the presence of small gaps in the Majorana spectrum and of two vison bands for h-driven hopping. We do, however, expect the same qualitative T dependence of the longitudinal mobility in this case, see Eq. (13) below, as long as T is larger than field-induced gaps in the Majorana spectrum. Furthermore, there will be a small transversal mobility arising from the Berry curvature of the bands.

We consider the limit, where the temperature T is smaller than the vison gap (thus that the density of visons is small). In this regime, we can describe the Majorana modes by a Dirac equation with velocity v_m. The scattering cross section of 2D Dirac electrons from a π flux is well known [42, 43] (see also App. B) and given by $\frac{d\sigma}{d\theta} = \frac{1}{2\pi k \sin^2(\theta/2)}$. Furthermore, we can use that the momentum transfer $\Delta p \sim T/v_m$ during a scattering process is small compared to the typical vison momentum $\sim \sqrt{T/W_v}/a$, where $W_v = 9|t_\Gamma|$ is the vison bandwidth and a the lattice constant. As shown in App. C, this allows to rewrite [44] the singular Boltzmann scattering kernel into a non-singular drift-diffusion equation in momentum space describing Brownian motion.

$$\partial_t f_{\boldsymbol{p}} + \boldsymbol{v}^v_{\boldsymbol{p}} \cdot \boldsymbol{F} \frac{df^0}{dE^v_{\boldsymbol{p}}} \approx D_p \left(\nabla^2_{\boldsymbol{p}} f_{\boldsymbol{p}} + \frac{1}{T} \boldsymbol{\nabla}_{\boldsymbol{p}} \left(\boldsymbol{v}^v_{\boldsymbol{p}} f_{\boldsymbol{p}} \right) \right), \tag{12}$$

where $f_{\boldsymbol{p}}$ is the vison distribution function, $v^v_{\boldsymbol{p}} = dE^v_{\boldsymbol{p}}/d\boldsymbol{p}$ the vison velocity and $D_p = 6T^3/v_m^2$ is the diffusion constant in momentum space, see App. C. The asymptotic behaviour of the mobility can then be calculated analytically

$$\mu(T) = \frac{D(T)}{T} = \begin{cases} \frac{18 t_\Gamma^2 v_m^2}{T^4} & \text{for } K \gg T \gg W_v \\ \frac{6 v_m^2}{T^2} & \text{for } T \ll W_v \end{cases}. \tag{13}$$

Remarkably, the low-temperature mobility $\mu(T)$ and therefore also the vison diffusion constant $D(T)$ are fully universal and completely independent of the vison dispersion, which follows from the scale invariance of the problem and the universal scattering cross section. Similar results (with different prefactors) exist for the problem of a vortex in a d-wave superconductor [41]. In Fig. 2 we show the mobility as function of T for different values of Γ.

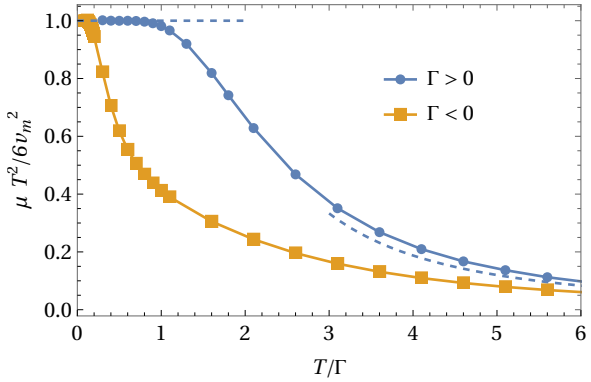

FIG. 2: Vison mobility, $\mu/(6v_m^2/T^2)$, in the ferromagnetic Kitaev model perturbed by a Γ term. μ is normalized to its low-T asymptotics and plotted as function of $T/|\Gamma|$ both for $\Gamma > 0$ and $\Gamma < 0$. Deviations from the universal low-T mobility are more pronounced for $\Gamma < 0$ at low T due to flat regions in the band structure close to the band minimum, see Fig. 1. The dashed lines indicate the low-T and high-T asymptotics, see Eq. (13).

1st order PT: AFM Kitaev –When evaluating the vison hopping rate, Eq. (9), for a antiferromagnetic Kitaev coupling, $K > 0$, we obtain the remarkable result that it vanishes exactly for both h and Γ perturbations. To understand the origin of this effect, it is useful to realize that a single vison hopping process arises from the interference of two contributions, $t_{ab} = A_1 + A_2$ due to two different terms in the Hamiltonian ΔH_1 and ΔH_2. For example, for the z-link shown in Fig. 3, $\Delta H_1 = \Gamma\sigma_i^x\sigma_j^y$ (or $\Delta H_1 = \frac{h}{\sqrt{3}}\sigma_i^z$) while $\Delta H_2 = \Gamma\sigma_i^y\sigma_j^x$ (or $\Delta H_2 = \frac{h}{\sqrt{3}}\sigma_j^z$). Importantly, these two terms are related by a reflection symmetry (dashed lines in Fig. 3), which ensures that $A_1 = \pm A_2$. To fix the sign, we observe that $\langle \Delta H_1 \Delta H_2\rangle = \langle \sigma_i^z\sigma_j^z\rangle$ is negative in the AFM Kitaev model while positive in the FM Kitaev model. This strongly suggests that $A_1 = -A_2$ in the AFM phase as we confirmed numerically by direct evaluation of Eq. (9): a destructive interference eliminates the leading vison hopping process.

$$t_h = t_\Gamma = 0. \tag{14}$$

This effect is reminiscent of the 'Aharonov-Bohm caging' describing the localization by destructive interference which is often induced in models with π-fluxes and nearest-neighbor hopping only [45, 46]. Note that longer-range hopping arising to quadratic order in h or Γ is still possible in our system.

Majorana assisted hopping – The perfect destructive interference, which prohibits vison motion linear in ΔH in the AFM case, is disturbed when the vison scatters from thermally excited Majorana fermions. Thus at $T > 0$ there will be a Majorana-assisted *incoherent* hopping process with rate W. As ΔH is small, we can use Fermi's golden-rule to compute the hopping rate W for a vison moving from site $\boldsymbol{R}_a$ to $\boldsymbol{R}_b$. The fact that the presence of the vison strongly disturbs the Majorana fermions makes this a non-standard calculation. We can use, however, that for $T \ll K$ the Majorana density is low and the calculation can be done in a continuum model describing the vison by a point-like π flux, see App. D for details.

$$W = 2\pi \sum_{k,k',l,l'} |\langle k', l', R_b|\Delta H|k, l, R_a\rangle|^2 n(\epsilon_k)\delta(\epsilon_k - \epsilon_{k'}) \tag{15}$$

Here l, l' are the angular momentum quantum numbers of the scattering wave functions, $n(\epsilon_k)$ is the Fermi function and $\epsilon_k = v_m k$ the dispersion of low-energy Majoranas. The hopping rate W induces a random walk on the vison lattice, from which the diffusion constant D and thus (via Einstein's relation) the mobility can be obtained. W and thus D are linear in T, see App. C, therefore we obtain a T-independent mobility

$$\mu(T) = \frac{D(T)}{T} \sim \begin{cases} \frac{\Gamma^2 a^4}{v_m^2} & \text{for } K \gg T \gg \sqrt{\Gamma K} \\ \frac{h^2 a^4}{v_m^2} & \text{for } K \gg T \gg \sqrt{hK} \end{cases} \tag{16}$$

for perturbations by Γ and h, respectively. The formula is valid only for rather high temperatures, because at lower T coherent second-order (longer-range) hopping processes set in giving rise to a bandwidth of order $W_v^{(2)} \sim \Gamma^2/K, h^2/K$. In the low-temperature regime, one can simply replace W_v and t_Γ by $W_v^{(2)}$ in Eq. (13) to obtain an estimate for the mobility.

The T-independent mobility of Eq. (16) is reminiscent of ohmic friction, but its physical origin (assisted hopping) is very different compared to, e.g., Landau damping.

Heisenberg interaction – Finally, we briefly discuss the effects of a small perturbation by a Heisenberg term, $\Delta H_J = J\sum_{ij} \boldsymbol{\sigma}_i\boldsymbol{\sigma}_j$. Applying ΔH_J to a single vison creates a state with three or five visons. Thus there is no vison hopping linear in J. While we have not performed a complete calculation to order J^2, we argue in App. E that single-vison hopping processes at order J^2 cancel by an interference effect very similar to the one discussed above for $K > 0$. An important difference is, however, that this destructive interference occurs for both signs of

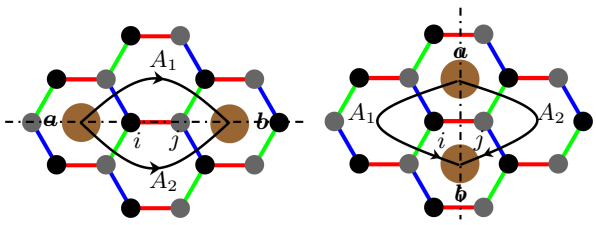

FIG. 3: Vison hopping processes induced by (a) ΔH_Γ (b) ΔH_h. The brown disks represent the visons (positions $\boldsymbol{R}_a$ and $\boldsymbol{R}_b$) and the black curves show different trajectories that interfere constructively (destructively) for FM (AFM) Kitaev interaction.

K. This suggests that coherent vison hopping induced by J occurs only to order J^4. In contrast, vison pairs can hop already to linear order in J as recently shown by Zhang *et al.* [32]. For single-vison hopping, however, we expect that Γ is much more important than J.

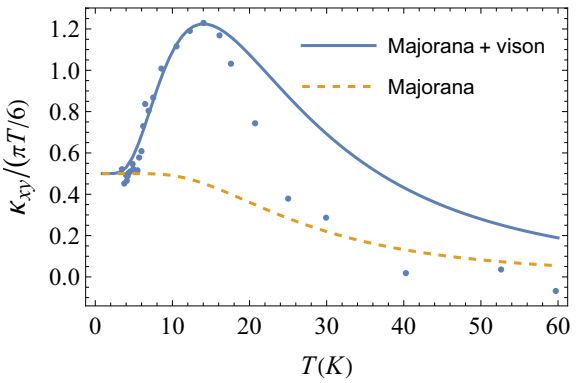

FIG. 4: Thermal Hall effect as function of temperature. Points: experimental data for α-$RuCl_3$ from Ref. [13] measured at 10 T ($\theta = -45°$, see Fig. 2D in Ref. [13]). Line: Fit to theory assuming two independent additive contributions from Majorana fermions (dashed line) and visons. Note that the theory is not valid for $T \gtrsim 15$ K as the vison density becomes too high in this regime, see App. F for details. Vison-Majorana scattering, not taken into account in the theory, may explain [47] why the experimental signal drops faster at higher T. Parameters: $E_0^v = 48$ K, $|t_h| = 9.6$ K, $K = -70$ K and $t_{AA}^m = 14$ K.

Thermal Hall effect – One of the most promising ways to detect *mobile* visons experimentally is to search for their signatures in heat transport [48]. Here we can use that our theory predicts vison bands with Chern numbers ± 1 in a magnetic field assuming FM Kitaev coupling. Thus occupying the lowest band thermally will give rise to an extra contribution to the thermal Hall effect. To calculate this effect, we assume that the vison bands are thermally occupied with the probability $e^{-\beta(E^v_{\alpha\boldsymbol{k}} - T\ln\sqrt{2})}$, where $E^v_{\alpha\boldsymbol{k}}$ is the vison dispersion in band $\alpha = 1, 2$ and the entropic correction $T\ln\sqrt{2}$ takes into account that the vison (to be identified with the Ising anyon excitation of the chiral spin liquid phase) carries a Majorana zero mode when the Majorana spectrum obtains a gap [1]. The resulting thermal Hall effect can then be calculated directly [16] from the Berry curvature of the bands, see App. F. We obtain a pronounced peak in κ_{xy}/T as function of T which turns out to have a similar amplitude and the same sign as the quantized contribution from the Majorana fermions. Remarkably, precisely such a contribution has been observed in the thermal Hall effect measurements on α-$RuCl_3$ [11, 13]: a large additive contribution to the quantized thermal Hall effect is found, which peaks around 14 K. In Fig. 4 we show the experimental data together with a fit to our calculation of $\kappa_{xy}(T)$, where we also included the contribution from Majorana fermions which is quantized at low T and drops for T larger than the field-induced gap in the Majorana spectrum. As the theory is based on the low-density limit for visons and does not take any vison-vison or vison-Majorana interactions into account, it is not valid in the high-temperature regime. Thus the precise shape of the peak not correctly reproduced. The existence of the large peak in κ_{xy} is, however, a clear signature of a mobile massive excitation with a Chern band which we identify with a dynamical vison. Here the extra degeneracy of the vison due to Majorana zero modes helps to reproduce the remarkably large amplitude of the experimentally observed peak reaching about 0.7 conductance quanta above the 0.5 Majorana plateau. A recent study by Go, Jung and Moon [49] finds that certain magnetic next-nearest-neighbor interactions treated within a Majorana-based mean field theory also produce massive excitations with Chern numbers and thus similar signatures in κ_{xy} are obtained in Ref. [49] with somewhat smaller amplitudes.

Discussion – Depending on temperature and the sign of the Kitaev coupling K, we find that a vison can either behave as a coherent quasiparticle with very large mobility or as an incoherent excitation with a small mobility. For antiferromagnetic Kitaev coupling interference effects eliminate all leading order vison-tunneling processes. This immediately explains why the antiferromagnetic Kitaev model is much more robust against perturbations by Γ or h than its ferromagnetic counterpart. In the ferromagnetic case the vison gap shrinks for increasing vison hopping, thus triggering a phase transition when the vison gap closes, see App. G for a more detailed analysis and a quantitative comparison to existing numerical studies.

Our theory provides a controlled calculation in the limit of weak perturbations to Kitaev models. As such it cannot be directly applied to materials like α-$RuCl_3$ where at zero magnetic field these perturbations induce magnetic order, thus destroying the spin liquid state. The observation of a half-integer quantized thermal Hall effect in this material [11–14] at a field of about 10 T, however, suggests that this field-induced phase is adiabatically connected to the physics of a ferromagnetic [10, 50–53] Kitaev model weakly perturbed by a magnetic field. Thus it is highly plausible that this phase also hosts a dynamical gauge field with vison bands characterized by Chern numbers. We interpret the experimentally observed [11, 13] peak on top of the quantized plateau as a smoking-gun signature of a dynamical vison with a topological band structure. Within this interpretation, we obtain a vison gap of the order of 20 K, a vison bandwidth in the same range and a separation of the two vison bands of roughly 40 K. Phonons can also provide an extra contribution to the thermal Hall effect, which, however, is predicted [16] to be rather small and is therefore very unlikely to explain the observed peak. Thermal excitations of Majorana fermions, in contrast, and also Majorana-vison scattering are expected to *reduce* κ_{xy} compared to the quantized value as has been shown numerically by Nasu, Yoshitake Motome [47] in a model with static visons. Majorana-vison scattering,

which has been ignored in our theoretical analysis of the Hall effect can, most likely, also explain why the experimental signal decays faster than the theoretical result at large T, see Ref. [47]. We thus conclude that the experimental observation provides strong evidence for the realization of one of the most profound concepts in modern solid state physics, the emergence of dynamical gauge fields, in $RuCl_3$.

For the future, it will be interesting to track both theoretically and experimentally the vison and its contribution to the thermal Hall effect upon approaching quantum phase transitions from a (chiral) quantum spin liquid to neighboring phases.

ACKNOWLEDGMENTS

We thank Simon Trebst, Martin Zirnbauer and, especially, Ciarán Hickey for numerous very helpful discussions. A.P.J is also grateful to Jinhong Park for useful discussions. This work was supported by the Deutsche Forschungsgemeinschaft (DFG) through CRC1238 (Project No. 277146847, project C02 and C04) and – under Germany's Excellence Strategy – by the Cluster of Excellence Matter and Light for Quantum Computing (ML4Q) EXC2004/1 390534769 and by the Bonn-Cologne Graduate School of Physics and Astronomy (BCGS).

[1] A. Kitaev, Anyons in an exactly solved model and beyond, Annals of Physics **321**, 2 (2006).
[2] T. Senthil and M. P. A. Fisher, Z_2 gauge theory of electron fractionalization in strongly correlated systems, Phys. Rev. B **62**, 7850 (2000).
[3] Y. Huh, M. Punk, and S. Sachdev, Optical conductivity of visons in Z_2 spin liquids close to a valence bond solid transition on the kagome lattice, Phys. Rev. B **87**, 235108 (2013).
[4] Z. Hao, Detecting nonmagnetic excitations in quantum magnets, Phys. Rev. B **85**, 174432 (2012).
[5] A. Kitaev, Fault-tolerant quantum computation by anyons, Annals of Physics **303**, 2 (2003).
[6] S. Trebst, Kitaev Materials (2017), arXiv:1701.07056 [cond-mat.str-el].
[7] J. Knolle, D. L. Kovrizhin, J. T. Chalker, and R. Moessner, Dynamics of a Two-Dimensional Quantum Spin Liquid: Signatures of Emergent Majorana Fermions and Fluxes, Phys. Rev. Lett. **112**, 207203 (2014).
[8] A. Banerjee, P. Lampen-Kelley, J. Knolle, C. Balz, A. A. Aczel, B. Winn, Y. Liu, D. Pajerowski, J. Yan, C. A. Bridges, A. T. Savici, B. C. Chakoumakos, M. D. Lumsden, D. A. Tennant, R. Moessner, D. G. Mandrus, and S. E. Nagler, Excitations in the field-induced quantum spin liquid state of α-$RuCl_3$, npj Quantum Materials **3**, 8 (2018).
[9] N. Janša, A. Zorko, M. Gomilšek, M. Pregelj, K. W. Krämer, D. Biner, A. Biffin, C. Rüegg, and M. Klanjšek, Observation of two types of fractional excitation in the Kitaev honeycomb magnet, Nature Physics **14** (2018).
[10] A. Banerjee, C. A. Bridges, J.-Q. Yan, A. A. Aczel, L. Li, M. B. Stone, G. E. Granroth, M. D. Lumsden, Y. Yiu, J. Knolle, S. Bhattacharjee, D. L. Kovrizhin, R. Moessner, D. A. Tennant, D. G. Mandrus, and S. E. Nagler, Proximate Kitaev quantum spin liquid behaviour in a honeycomb magnet, Nature Materials **15** (2016).
[11] Y. Kasahara, T. Ohnishi, Y. Mizukami, O. Tanaka, S. Ma, K. Sugii, N. Kurita, H. Tanaka, J. Nasu, Y. Motome, T. Shibauchi, and Y. Matsuda, "Majorana quantization and half-integer thermal quantum Hall effect in a Kitaev spin liquid", Nature **559** (2018).
[12] M. Yamashita, J. Gouchi, Y. Uwatoko, N. Kurita, and H. Tanaka, Sample dependence of half-integer quantized thermal Hall effect in the Kitaev spin-liquid candidate $\alpha-RuCl_3$, Phys. Rev. B **102**, 220404 (2020).
[13] T. Yokoi, S. Ma, Y. Kasahara, S. Kasahara, T. Shibauchi, N. Kurita, H. Tanaka, J. Nasu, Y. Motome, C. Hickey, S. Trebst, and Y. Matsuda, Half-integer quantized anomalous thermal Hall effect in the Kitaev material candidate α-$RuCl_3$, Science **373** (2021).
[14] J. A. N. Bruin, R. R. Claus, Y. Matsumoto, N. Kurita, H. Tanaka, and H. Takagi, Robustness of the thermal Hall effect close to half-quantization in a field-induced spin liquid state (2021), arXiv:2104.12184 [cond-mat.str-el].
[15] M. Ye, G. B. Halász, L. Savary, and L. Balents, Quantization of the Thermal Hall Conductivity at Small Hall Angles, Phys. Rev. Lett. **121**, 147201 (2018).
[16] Y. Vinkler-Aviv and A. Rosch, Approximately Quantized Thermal Hall Effect of Chiral Liquids Coupled to Phonons, Phys. Rev. X **8**, 031032 (2018).
[17] R. G. Pereira and R. Egger, Electrical Access to Ising Anyons in Kitaev Spin Liquids, Phys. Rev. Lett. **125**, 227202 (2020).
[18] J. Feldmeier, W. Natori, M. Knap, and J. Knolle, Local probes for charge-neutral edge states in two-dimensional quantum magnets, Phys. Rev. B **102**, 134423 (2020).
[19] M. Udagawa, S. Takayoshi, and T. Oka, Scanning Tunneling Microscopy as a Single Majorana Detector of Kitaev's Chiral Spin Liquid, Phys. Rev. Lett. **126**, 127201 (2021).
[20] E. J. König, M. T. Randeria, and B. Jäck, Tunneling Spectroscopy of Quantum Spin Liquids, Phys. Rev. Lett. **125**, 267206 (2020).
[21] W.-H. Kao, J. Knolle, G. B. Halász, R. Moessner, and N. B. Perkins, Vacancy-Induced Low-Energy Density of States in the Kitaev Spin Liquid, Phys. Rev. X **11**, 011034 (2021).

[22] J. Knolle, R. Moessner, and N. B. Perkins, Bond-Disordered Spin Liquid and the Honeycomb Iridate $H_3LiIr_2O_6$: Abundant Low-Energy Density of States from Random Majorana Hopping, Phys. Rev. Lett. **122**, 047202 (2019).

[23] T. Minakawa, Y. Murakami, A. Koga, and J. Nasu, Majorana-Mediated Spin Transport in Kitaev Quantum Spin Liquids, Phys. Rev. Lett. **125**, 047204 (2020).

[24] G. Khaliullin and G. Jackeli, Mott Insulators in the Strong Spin-Orbit Coupling Limit: From Heisenberg to a Quantum Compass and Kitaev Models, Physical Review Letters **102** (2009).

[25] S. M. Winter, Y. Li, H. O. Jeschke, and R. Valentí, Challenges in design of Kitaev materials: Magnetic interactions from competing energy scales, Phys. Rev. B **93**, 214431 (2016).

[26] S. Bhattacharjee, R. Moessner, and J. Knolle, Dynamics of a quantum spin liquid beyond integrability: The Kitaev-Heisenberg-Γ model in an augmented parton mean-field theory, Physical Review B **97** (2018).

[27] C. Hickey and S. Trebst, Emergence of a field-driven U (1) spin liquid in the Kitaev honeycomb model, Nature Communications **10**.

[28] J. Wang, B. Normand, and Z.-X. Liu, One Proximate Kitaev Spin Liquid in the $K-J-\Gamma$ Model on the Honeycomb Lattice, Phys. Rev. Lett. **123**, 197201 (2019).

[29] M. Gohlke, G. Wachtel, Y. Yamaji, F. Pollmann, and Y. B. Kim, Quantum spin liquid signatures in Kitaev-like frustrated magnets, Phys. Rev. B **97**, 075126 (2018).

[30] M. Gohlke, R. Moessner, and F. Pollmann, Dynamical and topological properties of the Kitaev model in a [111] magnetic field, Phys. Rev. B **98**, 014418 (2018).

[31] J. S. Gordon, A. Catuneanu, E. S. Sørensen, and H.-Y. Kee, Theory of the field-revealed Kitaev spin liquid, Nature communications **10**, 1 (2019).

[32] S.-S. Zhang, G. B. Halász, W. Zhu, and C. D. Batista, Variational study of the Kitaev-Heisenberg-Gamma model, Phys. Rev. B **104**, 014411 (2021).

[33] S.-S. Zhang, G. B. Halász, and C. D. Batista, Theory of the Kitaev model in a [111] magnetic field (2021), arXiv:2104.02892 [cond-mat.str-el].

[34] G. Baskaran, S. Mandal, and R. Shankar, Exact Results for Spin Dynamics and Fractionalization in the Kitaev Model, Phys. Rev. Lett. **98**, 247201 (2007).

[35] L. M. Robledo, Sign of the overlap of Hartree-Fock-Bogoliubov wave functions, Physical Review C **79**.

[36] L. M. Robledo, Technical aspects of the evaluation of the overlap of Hartree-Fock-Bogoliubov wave functions, Phys. Rev. C **84**, 014307 (2011).

[37] A. J. Willans, J. T. Chalker, and R. Moessner, Disorder in a Quantum Spin Liquid: Flux Binding and Local Moment Formation, Phys. Rev. Lett. **104**, 237203 (2010).

[38] W.-H. Kao, J. Knolle, G. B. Halász, R. Moessner, and N. B. Perkins, Vacancy-Induced Low-Energy Density of States in the Kitaev Spin Liquid, Phys. Rev. X **11**, 011034 (2021).

[39] G. Volovik, Comment on vortex mass and quantum tunneling of vortices, Journal of Experimental and Theoretical Physics Letters **65**, 217 (1997).

[40] N. B. Kopnin and V. M. Vinokur, Dynamic Vortex Mass in Clean Fermi Superfluids and Superconductors, Phys. Rev. Lett. **81**, 3952 (1998).

[41] P. Nikolić and S. Sachdev, Effective action for vortex dynamics in clean d-wave superconductors, Phys. Rev. B **73**, 134511 (2006).

[42] S. Ganeshan, M. Kulkarni, and A. C. Durst, Quasiparticle scattering from vortices in d-wave superconductors. II. Berry phase contribution, Phys. Rev. B **84**, 064503 (2011).

[43] Y. Aharonov and D. Bohm, Significance of Electromagnetic Potentials in the Quantum Theory, Phys. Rev. **115**, 485 (1959).

[44] P. C. Howell, A. Rosch, and P. J. Hirschfeld, Relaxation of Hot Quasiparticles in a d-Wave Superconductor, Phys. Rev. Lett. **92**, 037003 (2004).

[45] J. Vidal, R. Mosseri, and B. Douçot, Aharonov-Bohm Cages in Two-Dimensional Structures, Phys. Rev. Lett. **81**, 5888 (1998).

[46] M. Rizzi, V. Cataudella, and R. Fazio, Phase diagram of the Bose-Hubbard model with $\mathbb{T}_3$ symmetry, Phys. Rev. B **73**, 144511 (2006).

[47] J. Nasu, J. Yoshitake, and Y. Motome, Thermal Transport in the Kitaev Model, Phys. Rev. Lett. **119**, 127204 (2017).

[48] Y. Qi, C. Xu, and S. Sachdev, Dynamics and Transport of the Z_2 Spin Liquid: Application to $\kappa-(ET)_2Cu_2(CN)_3$, Phys. Rev. Lett. **102**, 176401 (2009).

[49] A. Go, J. Jung, and E.-G. Moon, Vestiges of Topological Phase Transitions in Kitaev Quantum Spin Liquids, Phys. Rev. Lett. **122**, 147203 (2019).

[50] R. Yadav, N. A. Bogdanov, V. M. Katukuri, S. Nishimoto, J. van den Brink, and L. Hozoi, Kitaev exchange and field-induced quantum spin-liquid states in honeycomb $\alpha RuCl_3$, Scientific Reports **6**.

[51] S. M. Winter, Y. Li, H. O. Jeschke, and R. Valentí, Challenges in design of Kitaev materials: Magnetic interactions from competing energy scales, Phys. Rev. B **93**, 214431 (2016).

[52] J. A. Sears, L. E. Chern, S. Kim, P. J. Bereciartua, S. Francoual, Y. B. Kim, Y.-J. Kim, L. E. Chern, S. Kim, P. J. Bereciartua, S. Francoual, Y. B. Kim, and Y.-J. Kim, Ferromagnetic Kitaev interaction and the origin of large magnetic anisotropy in α-$RuCl_3$, Nature Physics **16** (2020).

[53] Y. S. Hou, H. J. Xiang, and X. G. Gong, Unveiling magnetic interactions of ruthenium trichloride via constraining direction of orbital moments: Potential routes to realize a quantum spin liquid, Phys. Rev. B **96**, 054410 (2017).

[54] F. L. Pedrocchi, S. Chesi, and D. Loss, Physical solutions of the Kitaev honeycomb model, Phys. Rev. B **84**, 165414 (2011).

[55] M. Vojta and F. Zschocke, Physical states and finite-size effects in Kitaev's honeycomb model: Bond disorder, spin excitations, and NMR line shape, Physical Review B **92** (2015).

[56] M. Wimmer, Algorithm 923: Efficient Numerical Computation of the Pfaffian for Dense and Banded Skew-Symmetric Matrices, ACM Trans. Math. Softw. **38**, 10.1145/2331130.2331138 (2012).

[57] O. Vafek, A. Melikyan, and Z. Tešanović, Quasiparticle Hall transport of d-wave superconductors in the vortex state, Phys. Rev. B **64**, 224508 (2001).

[58] Reif, F. (1965). Fundamentals of statistical and thermal physics. New York: McGraw-Hill.

[59] L. Zhang, Berry curvature and various thermal Hall effects, New Journal of Physics **18**.

[60] J. G. Rau, E. K.-H. Lee, and H.-Y. Kee, Generic Spin

Model for the Honeycomb Iridates beyond the Kitaev Limit, Phys. Rev. Lett. **112**, 077204 (2014).
[61] H.-Y. Lee, R. Kaneko, L. E. Chern, T. Okubo, Y. Yamaji, N. Kawashima, Y. B. Kim, R. Kaneko, L. E. Chern, T. Okubo, Y. Yamaji, N. Kawashima, Y. B. Kim, R. Kaneko, L. E. Chern, T. Okubo, Y. Yamaji, N. Kawashima, and Y. B. Kim, Magnetic field induced quantum phases in a tensor network study of Kitaev magnets, Nature Communications **11**.
[62] M. Gohlke, L. E. Chern, H.-Y. Kee, and Y. B. Kim, Emergence of nematic paramagnet via quantum order-by-disorder and pseudo-Goldstone modes in Kitaev magnets, Phys. Rev. Research **2**, 043023 (2020).
[63] J. c. v. Chaloupka, G. Jackeli, and G. Khaliullin, Zigzag Magnetic Order in the Iridium Oxide Na_2IrO_3, Phys. Rev. Lett. **110**, 097204 (2013).

Appendix A: Matrix element calculation

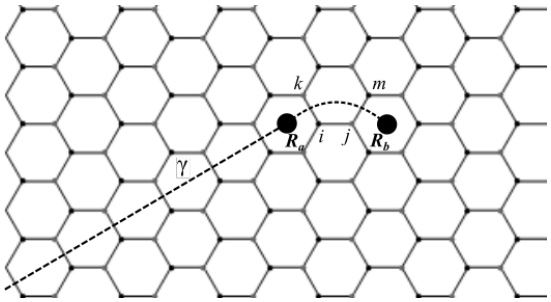

FIG. 5: Schematic showing the gauge configurations for the vison states used in the computation of matrix elements (Eq. A2). In a periodic system, a vison at R_a is created by flipping the u_{ij} variables along the dashed line. The other end of the line carries another vison far separated.

In this section, we describe the Pfaffian method [35] for calculating hopping matrix elements, Eq. (9), which involve the overlap of different Bogoliubov vacua. The starting point of our analysis is the many-body wave function, Eq. (8) in the main text, of Majorana fermions scattering from a localized vison (or a pair of visons, see below),

$$|\Phi(\boldsymbol{R}_a)\rangle = \hat{P}\prod_{l\in\gamma}\chi_l^\dagger\,|0_\chi\rangle\,|M_0(\boldsymbol{R}_a,\mathcal{G}_a)\rangle\,. \tag{A1}$$

The gauge configuration is expressed in terms of the bond fermion wave-functions, where γ is a semi-infinite string of x links flipped by the action of $\chi_l^\dagger$ on the bond fermion vacuum $|0_\chi\rangle$. $|M_0(\boldsymbol{R}_a,\mathcal{G}_a)\rangle$ is the many-body ground state wave function of the matter fermions in the chosen gauge. Note that for $|\Phi_0(\boldsymbol{R}_a)\rangle$ we have the freedom to choose any gauge configuration but the projection operator ensures gauge invariance. It is easy to see that the most convenient choice to relate two vison wave functions located at positions $\boldsymbol{R}_a$ and $\boldsymbol{R}_b$, see Fig. 5, is $|\mathcal{G}_b\rangle = \chi^\dagger_{\langle mj\rangle_y}\chi^\dagger_{\langle ik\rangle_x}|\mathcal{G}_a\rangle$. Eliminating the gauge sector by contracting the bond fermions, Eq. (9) for Γ perturbation becomes

$$\begin{aligned} t^\Gamma_{ab} &= \Gamma\,\langle M_0(\boldsymbol{R}_a,\mathcal{G}_a)|\,\langle\mathcal{G}_a|\,(b_i^y b_j^x c_i c_j + b_i^x b_j^y c_i c_j \hat{D}_j\hat{D}_i)\,|\mathcal{G}_b\rangle\,|M_0(\boldsymbol{R}_b,\mathcal{G}_b)\rangle \\ &= \Gamma\,\langle M_0(\boldsymbol{R}_a,\mathcal{G}_a)|\,(-ic_ic_j-1)\,|M_0(\boldsymbol{R}_b,\mathcal{G}_b)\rangle \end{aligned} \tag{A2}$$

Similarly, one can show that for ΔH_h, the matrix element for hopping across the $\langle ij\rangle_z$ link can be written as

$$t^h_{ab} = \langle M_0(\boldsymbol{R}_a,\mathcal{G}_a)|\,(-i+c_ic_j)\,|M_0(\boldsymbol{R}_b,\mathcal{G}_b)\rangle \tag{A3}$$

where we used a gauge transformation for the spin operator which is equivalent to rewriting $\sigma^z = -i\sigma^x\sigma^y$. The positions R_a and R_b are defined in Fig. 3b. We used the following decomposition of the projection operator that relates it to the total fermionic parity (bond and matter

fermions) [54].

$$\hat{P} = \hat{P}' \frac{(1 + \prod_i \hat{D}_i)}{2} = \hat{P}' \frac{1 + (-1)^{\theta + N_\chi + N_f}}{2} \tag{A4}$$

where $\theta \in \mathbb{Z}$ is a geometric factor that depends on the lattice boundary conditions, see Ref. [55] for details. This helps to avoid choosing an unphysical state while evaluating Eq. (A2) and Eq. (A3) (for finite systems) which would otherwise give zero as $\hat{P}$ projects away any unphysical state. Hence we choose the gauge configuration $(\mathcal{G}_a, \mathcal{G}_b)$ such that the ground states are physical by calculating the fermionic parities explicitly using the methods discussed in Refs. [54, 55].

For our calculation we use periodic boundary conditions with *two* visons placed at a large distance. The position of the second vison is always kept fixed (with its position coordinate suppressed in Eq. (A1)) while the position of the first vison is denoted by $\boldsymbol{R}_a$. To compute the matrix elements, we first diagonalize the Majorana Hamiltonian with a vison at a reference position $\boldsymbol{R}_d$, $\boldsymbol{R}_a$ and $\boldsymbol{R}_b$ using suitable gauge configurations. The corresponding Bogoliubov transformations are of the form

$$\begin{pmatrix} X^{(a)*} & Y^{(a)*} \\ Y^{(a)} & X^{(a)} \end{pmatrix} \begin{pmatrix} f \\ f^\dagger \end{pmatrix} = \begin{pmatrix} a \\ a^\dagger \end{pmatrix} \tag{A5}$$

for $\boldsymbol{R}_a$ and the $a \leftrightarrow b, d$ for $\boldsymbol{R}_b$ and $\boldsymbol{R}_d$ respectively. We define a reference vacuum $\left|\tilde{0}\right\rangle$ and fermionic operator d_i with $d_i \left|\tilde{0}\right\rangle = 0$ [36]. Importantly, this state must have the same total fermion parity as the two ground states of our interest and must be physical. One can choose this to be, say the ground state of a third vison position. The Bogoliubov operators a, which diagonalize the Kitaev model for a vison located at position $\boldsymbol{R}_a$ can be related to d by unitary matrices (similarly for $\boldsymbol{R}_b$).

$$\begin{pmatrix} \mathcal{X}^{(a)*} & \mathcal{Y}^{(a)*} \\ \mathcal{Y}^{(a)} & \mathcal{X}^{(a)} \end{pmatrix} \begin{pmatrix} d \\ d^\dagger \end{pmatrix} = \begin{pmatrix} a \\ a^\dagger \end{pmatrix} \tag{A6}$$

with $\mathcal{X}^{(a)*} = Y^{(a)} Y^{(d)\dagger} + X^{(a)} X^{(d)\dagger}$ and $\mathcal{Y}^{(a)*} = Y^{(a)} X^{(d)\dagger} + X^{(a)} Y^{(d)\dagger}$.

We can now express both $|M_0(R_a, \mathcal{G}_a)\rangle$ and $|M_0(\boldsymbol{R}_b, \mathcal{G}_b)\rangle$ in the following Thouless form [7, 35],

$$|M(\boldsymbol{R}_a, \mathcal{G}_a)\rangle = \left| \det\left(\mathcal{X}^{(a)}\right)^{\frac{1}{2}} \right| e^{-\frac{1}{2} d^\dagger Z^{(a)} d^\dagger} \left|\tilde{0}\right\rangle, \tag{A7}$$

with $Z^{(a)} = \left(\mathcal{X}^{(a)^{-1}} \mathcal{Y}^{(a)}\right)^*$. Matrix elements of the form needed for Eq. (A2) and (A3) can be computed using $d(d^\dagger)$ operators grouped into $(\tilde{d}_1 ... \tilde{d}_{2N}) = (d_1^\dagger ... d_N^\dagger d_1 ... d_N)$. Matrix elements of $\tilde{d}_m \tilde{d}_n$ can be computed using a coherent state path integral technique to give

$$\begin{aligned} &\langle M_0(\boldsymbol{R}_a, \mathcal{G}_a)| \, \tilde{d}_m \tilde{d}_n \, |M_0(\boldsymbol{R}_b, \mathcal{G}_b)\rangle \\ &\qquad = (-1)^{N(N+1)} \mathrm{Pf}(\mathbb{X}) \, \mathrm{Pf}(\mathbb{X}_{\{m,n\}}) \end{aligned} \tag{A8}$$

where Pf denotes the Pfaffian and $\mathbb{X}$ is a $2N \times 2N$ skew-symmetric matrix defined using $Z^{(a)}$ and $Z^{(b)}$,

$$\mathbb{X} = \begin{pmatrix} -Z^{(b)^*} & -I \\ I & Z^{(a)} \end{pmatrix}. \tag{A9}$$

where $\mathbb{X}_{\{m,n\}} = \begin{pmatrix} 0 & \mathbb{X}_{mn} \\ \mathbb{X}_{nm} & 0 \end{pmatrix}$ is a 2×2 matrix. Pfaffians were computed using the algorithm developed by Wimmer [56].

Appendix B: Scattering from a static vison

In this section we briefly review the scattering of low-energy Majorana degrees of freedom from a single, static vison. We will need the result to compute the mobility of mobile visons in the next section, App. C. At low energies the matter Majoranas, c, are described by Dirac equation with velocity $v_m = \sqrt{3}|K|/2$ at momenta $\boldsymbol{K}$ and $\boldsymbol{K}'$. Using the property $c_k = c_{-k}^\dagger$, we can combine the two Majorana cones into one single Dirac cone at $\boldsymbol{K}$ and restrict the momenta to half-Brillouin zone. Expanding around the momentum $\boldsymbol{K}$ one obtains in radial coordinates

$$\tilde{H}_{\boldsymbol{K}} = v_m \begin{pmatrix} 0 & ie^{i\theta}\left(\partial_r + \frac{i}{r}\partial_\theta\right) \\ ie^{-i\theta}\left(\partial_r - \frac{i}{r}\partial_\theta\right) & 0 \end{pmatrix} \tag{B1}$$

The vison is described as a point-like magnetic flux with flux π located at the origin of the coordinate system. We use a gauge where the presence of the flux can be absorbed into antiperodic boundary conditions in θ direction, $\psi(\theta) = -\psi(\theta + 2\pi)$. This is equivalent to a singular gauge often used in vortex scattering problems [57]. The scattering solutions can be obtained by solving a second order Bessel differential equation

$$\tilde{\psi}_{s,l,k}(r) = \begin{cases} \sqrt{\frac{k}{4\pi}} \begin{pmatrix} s^{\frac{1}{2}} J_{-l+\frac{1}{2}}(kr) e^{i(l-\frac{1}{2})\theta} \\ -s^{-\frac{1}{2}} i J_{-l-\frac{1}{2}}(kr) e^{i(l+\frac{1}{2})\theta} \end{pmatrix}, & l \leq 0 \\ \sqrt{\frac{k}{4\pi}} \begin{pmatrix} s^{\frac{1}{2}} J_{l-\frac{1}{2}}(kr) e^{i(l-\frac{1}{2})\theta} \\ s^{-\frac{1}{2}} i J_{l+\frac{1}{2}}(kr) e^{i(l+\frac{1}{2})\theta} \end{pmatrix}, & l > 0 \end{cases} \tag{B2}$$

where $s = \pm 1$ labels the positive and negative energy states respectively.

The case of $l = 0$ is special. The wave function weakly diverges at the origin as $r^{-\frac{1}{2}}$ and thus is a quasi-localized state [21]. The well-known scattering cross-section can be obtained as [42, 43]

$$\frac{d\sigma}{d\varphi} = \frac{1}{2\pi k \sin^2 \varphi}, \qquad \varphi \neq 0 \tag{B3}$$

where φ is the angle between incoming and outgoing beam.

Appendix C: Mobility of a vison

To discuss the mobility of a a single mobile vison, we use the language of a Boltzmann equation for the momentum distribution function $f_{\boldsymbol{p}} = f^0_{\boldsymbol{p}} + \delta f_{\boldsymbol{p}}$ of the vison. In the presence of an external force $\boldsymbol{F}$ acting on the vison, the linearized Boltzmann equation reads

$$\boldsymbol{F}\cdot\boldsymbol{v}^v_{\boldsymbol{p}}\frac{\partial f^0_{\boldsymbol{p}}}{\partial E^v_{\boldsymbol{p}}} = \int \tilde{M}_{\boldsymbol{p}\boldsymbol{p}'}\delta f_{\boldsymbol{p}'}\frac{d^2p'}{(2\pi)^2} \tag{C1}$$

Here the equilibrium distribution function of the gapped vison, $f^0_{\boldsymbol{p}} = c\, e^{-\beta E^v_{\boldsymbol{p}}}$, is given by a Boltzmann distribution as we work in the low-density limit and c is a normalization constant which will drop out in the final result. $E^v_{\boldsymbol{p}}$ is the dispersion of the vison, $\boldsymbol{v}^v_{\boldsymbol{p}} = \partial E^v_{\boldsymbol{p}}/\partial \boldsymbol{p}$ its velocity. The scattering rate from momentum $\boldsymbol{p}'$ to momentum $\boldsymbol{p}$ is determined from

$$M_{\boldsymbol{p},\boldsymbol{p}'} = \int \frac{d^2k}{(2\pi)^2}\frac{d^2k'}{(2\pi)^2} W^{\boldsymbol{p}}_{\boldsymbol{k},\boldsymbol{k}'}\; n^0_k(1-n^0_{k'}) \\ \delta(\boldsymbol{k}+\boldsymbol{p}-\boldsymbol{k}'-\boldsymbol{p}')\delta(\epsilon_{\boldsymbol{k}} + E^v_{\boldsymbol{p}'} - \epsilon_{\boldsymbol{k}'} - E^v_{\boldsymbol{p}}). \tag{C2}$$

with $\tilde{M}_{\boldsymbol{p}\boldsymbol{p}'} = M_{\boldsymbol{p}\boldsymbol{p}'} - \delta(\boldsymbol{p}-\boldsymbol{p}')\int M_{\boldsymbol{p}'\boldsymbol{p}}d^2p'$, where the second term describes the out-scattering from $\boldsymbol{p}$ to an arbitrary momentum $\boldsymbol{p}'$. As we consider a single vison embedded by many thermally excited Majorana modes, we can assume that the latter stay in equilibrium. Thus n^0_k is the Fermi distribution function in equilibrium. We consider the case where the Majorana dispersion arises from a small Γ term and we focus on the limit $T \ll K$. Thus, we can approximate the Majorana dispersion by $\epsilon_{\boldsymbol{k}} \approx v_m|\boldsymbol{k}|$. The transition rates $W^{\boldsymbol{p}}_{\boldsymbol{k},\boldsymbol{k}'}$ are discussed below.

We use the ansatz $\delta f_{\boldsymbol{p}} = \frac{\partial f_0}{\partial E^v_{\boldsymbol{p}}}\phi_{\boldsymbol{p}}$, where $\phi_{\boldsymbol{p}}$ is a smooth function in momentum and obtain

$$\boldsymbol{F}\cdot\boldsymbol{v}^v_{\boldsymbol{p}} = \int \tilde{M}_{\boldsymbol{p}\boldsymbol{p}'}e^{\beta(E^v_{\boldsymbol{p}}-E^v_{\boldsymbol{p}'})}\phi_{\boldsymbol{p}'}\frac{d^2p'}{(2\pi)^2} \tag{C3}$$

A substantial simplification of this matrix equation occurs because (i) the vison velocities are much smaller than Majorana velocities and (ii) due to $T \ll K$ the typical momenta of the Majorana modes, $\sim k_BT/v_m$, are small. Due to energy and momentum conservation, therefore the typical vison momentum transfer, $|\boldsymbol{p}-\boldsymbol{p}'| \sim k_BT/v_m$, is also small. Therefore one can expand the smoothly varying function $\phi_{\boldsymbol{p}'}$ and also $E^v_{\boldsymbol{p}} - E_{\boldsymbol{p}'}$ in the momentum difference retaining only the leading order terms. A similar approach has, for example, been used to describe the relaxation of high-energy quasiparticle in d-wave superconductors [44]. Thus, we arrive at

$$\boldsymbol{v}^v_{\boldsymbol{p}}\cdot\boldsymbol{F} \approx \int \tilde{M}_{\boldsymbol{p}\boldsymbol{p}'}e^{-\beta\boldsymbol{v}^v_{\boldsymbol{p}}(\boldsymbol{p}'-\boldsymbol{p})}\Big(\phi_{\boldsymbol{p}} + (\boldsymbol{p}'-\boldsymbol{p})\cdot\nabla_{\boldsymbol{p}}\phi_{\boldsymbol{p}}) \\ + \frac{(p'_i-p_i)(p'_j-p_j)}{2}\partial_{p_i}\partial_{p_j}\phi_{\boldsymbol{p}}\Big)\frac{d^2p'}{(2\pi)^2} \tag{C4}$$

The zeroth order terms vanish exactly due to the outscattering term in $\tilde{M}$. In the limit of vanishing vison bandwidth, $\boldsymbol{v}^v_{\boldsymbol{p}} \to 0$, also the second term vanishes as $\tilde{M}_{\boldsymbol{p},\boldsymbol{p}'}$ is only a function of $|\boldsymbol{p}-\boldsymbol{p}'|$ in this case. Therefore, we have to compute this term to linear order in $\boldsymbol{v}^v_{\boldsymbol{p}}$, while this is not necessary for the second-order term. Thus we arrive at the following drift-diffusion equation in momentum space

$$\partial_t\phi_{\boldsymbol{p}} + \boldsymbol{v}^v_{\boldsymbol{p}}\cdot\boldsymbol{F} \approx D_p\nabla^2_{\boldsymbol{p}}\phi_{\boldsymbol{p}} + \gamma\,\boldsymbol{v}^v_{\boldsymbol{p}}\cdot\boldsymbol{\nabla}_{\boldsymbol{p}}\phi_{\boldsymbol{p}} \tag{C5}$$

with yet undetermined prefactors D_p and γ. The ratio of γ and D_p can be determined without any microscopic calculation by demanding that Eq. (C5) obeys particle number conservation for arbitrary $\phi_{\boldsymbol{p}}$. From this condition, we derive $\gamma = -D_p/T$ and obtain

$$\partial_t\phi_{\boldsymbol{p}} + \boldsymbol{v}^v_{\boldsymbol{p}}\cdot\boldsymbol{F} \approx D_p\left(\nabla^2_{\boldsymbol{p}}\phi_{\boldsymbol{p}} - \frac{1}{T}\,\boldsymbol{v}^v_{\boldsymbol{p}}\cdot\boldsymbol{\nabla}_{\boldsymbol{p}}\phi_{\boldsymbol{p}}\right) \tag{C6}$$

or, after rewriting the result in terms of the vison distribution function $f_{\boldsymbol{p}}$ we obtain the equivalent equation

$$\partial_t f_{\boldsymbol{p}} + \boldsymbol{v}^v_{\boldsymbol{p}}\cdot\boldsymbol{F}\frac{df^0}{dE^v_{\boldsymbol{p}}} \approx D_p\left(\nabla^2_{\boldsymbol{p}}f_{\boldsymbol{p}} + \frac{1}{T}\,\boldsymbol{\nabla}_{\boldsymbol{p}}\left(\boldsymbol{v}^v_{\boldsymbol{p}}f_{\boldsymbol{p}}\right)\right). \tag{C7}$$

The two equations (C6) and (C7) describe the Brownian motion of the vison. There is a frictional force proportional to $-\boldsymbol{v}^v_{\boldsymbol{p}}$ which slows the vison down. This dissipation is necessarily accompanied by fluctuations: random forces due to vison-Majorana scattering lead to a diffusion in momentum space.

Due to the momentum dependence of the drift term, Eq. (C6) cannot be solved analytically but we obtain a numerical solution by Fourier transformation followed by a matrix inversion. In the low-T limit it is important to take a sufficient number of Fourier components into account as $\Phi_{\boldsymbol{p}}$ develops features with a width $\sim\sqrt{T}$.

Analytically, one can solve the the drift-diffusion equation for $T \gg W_v$ simply by ignoring the drift term proportional to $v^v_{\boldsymbol{p}}$ and by integrating the dispersion twice maintaining periodic boundary conditions. In the low-T limit, $T \ll W_v$, the stationary equation is approximately solved by $\phi_{\boldsymbol{p}} = -\frac{T}{D_p}\boldsymbol{F}\cdot\boldsymbol{p}$. The periodicity of $\phi_{\boldsymbol{p}}$ is thereby restored by a jump of the distribution function far away from the band minimum close to points where $\boldsymbol{F}\cdot v^v_{\boldsymbol{p}}$ vanishes.

The mobility μ of the vison is computed from

$$\langle\boldsymbol{v}^v_{\boldsymbol{p}}\rangle = \mu\,\boldsymbol{F} \\ \langle\boldsymbol{v}^v_{\boldsymbol{p}}\rangle = \frac{1}{N_v}\int\frac{d^2p}{(2\pi)^2}\boldsymbol{v}^v_{\boldsymbol{p}}\frac{\partial f_0}{\partial E^v_{\boldsymbol{p}}}\phi_{\boldsymbol{p}} \tag{C8}$$

with $N_v = \int f^0_{\boldsymbol{p}}\frac{d^2p}{(2\pi)^2}$.

We can now use the above described asymptotic solutions for $\phi_{\boldsymbol{p}}$ to calculate analytically the asymptotic

behavior of the mobility. We obtain

$$\mu \approx \begin{cases} \frac{3t^2}{D_p T} & \text{for } T \gg W_v \\ \frac{T}{D_p} & \text{for } T \ll W_v \end{cases} \tag{C9}$$

where t is the hopping matrix element of the vison.

The remaining task is to calculate the temperature dependence of the diffusion constant in momentum space, D_p. By definition D_p is independent of the vison dispersion, therefore its T dependence is a simple power law in this low T regime. This can be obtained in the following way. A two-dimensional Dirac equation has a linear density of states and therefore the density n_m of thermally excited Majorana fermions is proportional to T^2/v_m^2, where v_m is the velocity. The diffusion constant in momentum space is obtained from $(\delta k)^2/\tau$, where $\delta k \sim T/v_m$ is the typical momentum transfer in a scattering event. The scattering time is estimated from $\sigma v_m \tau n_m \sim 1$, where σ is the transport scattering cross section which scales with $1/k$, Eq. (B3), resulting in an extra factor v_m/T, and thus $1/\tau \sim T$. Combining these factors one obtains

$$D_p \sim \frac{T^3}{v_m^2}. \tag{C10}$$

To obtain the correct prefactors, one has to express the transition matrix $W_{\boldsymbol{k},\boldsymbol{k}'}$ in Eq. (C2) by the differential cross section for vison-Majorana scattering which is given in Eq. (B3). The two quantities are related by [58]

$$\frac{d^2p'}{(2\pi)^2}\frac{d^2k'}{(2\pi)^2} W_{\boldsymbol{k},\boldsymbol{k}'}(2\pi)^2\delta(\boldsymbol{k}+\boldsymbol{p}-\boldsymbol{k}'-\boldsymbol{p}')2\pi\delta(\epsilon_{\boldsymbol{k}}-\epsilon_{\boldsymbol{k}'}) \approx v_m d\theta_{\boldsymbol{k},\boldsymbol{k}'}\frac{d\sigma(k,\theta_{\boldsymbol{k},\boldsymbol{k}'})}{d\theta_{\boldsymbol{k},\boldsymbol{k}'}} \tag{C11}$$

This gives, using Eq. (C4)

$$D_p = v_m \int \frac{d^2k}{(2\pi)^2} d\theta_{\boldsymbol{k},\boldsymbol{k}'} k^2 \left(1-\cos\theta_{\boldsymbol{k},\boldsymbol{k}'}\right) \frac{d\sigma(k,\theta_{\boldsymbol{k},\boldsymbol{k}'})}{d\theta_{\boldsymbol{k},\boldsymbol{k}'}} n(\epsilon_k)(1-n_{\epsilon_{k'}}) = \frac{T^3}{6v_m^2} \tag{C12}$$

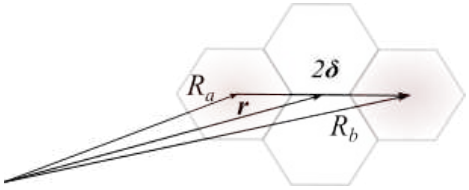

FIG. 6: Position vectors of vison used in the calculation of the assisted hopping rate due to a Γ perturbation. $\boldsymbol{r}$ is the position vector of the unit cell chosen to be a z bond.

This fixes the prefactor in Eq. (C10) in the limit where the vison mass is large. Thus it allows to compute analytically the exact mobility of the vison both in the low- and high-temperature regime using Eq. (C9).

Appendix D: Assisted hopping rate

In this section we calculate the mobility in the antiferromagnetic Kitaev model perturbed by Γ, similar results apply for a perturbation by a magnetic field, see below. In this section we use $\boldsymbol{r}$ to label unit cells and A and B to refer to the atom on sublattice A and B within the unit cell.

Consider $\Delta H_\Gamma = \Gamma(\sigma^x_{\boldsymbol{r},A}\sigma^y_{\boldsymbol{r},B} + \sigma^y_{\boldsymbol{r},A}\sigma^x_{\boldsymbol{r},B})$ with $\boldsymbol{r}$ being the coordinate of the center of the z-bond. This term induces a hopping of a vison along a z bond as shown in the Fig. 6. ΔH_Γ can be written as

$$\Delta H_\Gamma = \Gamma\left[b^x_{\boldsymbol{r},A}b^y_{\boldsymbol{r},B}\left(c^A_{\boldsymbol{r}} - ic^B_{\boldsymbol{r}}\right)\left(c^A_{\boldsymbol{r}} + ic^B_{\boldsymbol{r}}\right)\right] \tag{D1}$$

where we fixed $ib^z_{\boldsymbol{r},A}b^z_{\boldsymbol{r},B} = 1$ for the two single vison states. The $b^{x/y}_{\boldsymbol{r},A/B}$ operators realize the hopping of a bare vison and thus can be simply contracted in the matrix element calculation as we did in Appendix A, see Eq. (A2). The remaining terms affect the matter Majorana sector which we will treat in the low-energy long-wavelength approximation by replacing the c operators with their continuum fields.

$$c^A_{\boldsymbol{r}} = \int d^2r' w(\boldsymbol{r}') e^{\pm i\frac{\pi}{4}} \psi_A(\boldsymbol{r}'+\boldsymbol{r}) + h.c \tag{D2}$$

$w(\boldsymbol{r})$ is a "Wannier function" defining an effective cut-off of the low-energy theory. The position of the unit cell is $\boldsymbol{r} = \boldsymbol{R}_a + \boldsymbol{\delta} = \boldsymbol{R}_b - \boldsymbol{\delta}$ which means that the vison hops by the vector $2\boldsymbol{\delta}$, see Fig. 6.

We have shown that the ground-state matrix elements vanish for antiferromagnetic Kitaev coupling. Therefore, we now consider initial and final states, with a single fermionic excitation above the ground state, which we denote by $|M_n(\boldsymbol{R}_a)\rangle$. Here $n = \{s, l, k\}$ labels the eigenstates with quantum numbers $s = \pm$ labels particle/hole, $l \in \mathbb{Z}$ the angular momentum, and energy $\epsilon(k) = v_m k$. Those states will dominate in the low-T limit when the density of thermally excited Majorana states is low. Thus we need to compute for Eq. (15) the following matrix el-

ements

$$\tilde{w}^{ab}(m;n) = \langle M_n(\boldsymbol{R}_a)| \left(c^A_{\boldsymbol{r}} - ic^B_{\boldsymbol{r}}\right)\left(c^A_{\boldsymbol{r}} + ic^B_{\boldsymbol{r}}\right)|M_m(\boldsymbol{R}_b)\rangle\,. \tag{D3}$$

In the continuum theory, we implement the π flux carried by a vison as a branch cut that imposes anti-periodic boundary conditions for the Majorana wavefunctions, see App. B. As a next step, we expand the field operators in eigenstates of the scattering problem

$$\psi_{A/B}(\boldsymbol{r}-\boldsymbol{R}_a) = \sum_l \int \frac{dk}{2\pi}\sqrt{\pi k}\,(a_{+,k,l} - ia_{-,k,l})\left(f^{A/B}_{l,k}(\boldsymbol{r}-\boldsymbol{R}_a)\right)^* \tag{D4}$$

Here $a_{+,k,l}(a_{-,k,l})$ denote the eigen-modes with $\epsilon_k > 0$ ($\epsilon_k < 0$).

$$f^A_{l,k}(\boldsymbol{r}) = \begin{cases} J_{-l+\frac{1}{2}}e^{l-\frac{1}{2}\theta}e^{iK\cdot r} & l\le 0 \\ J_{l-\frac{1}{2}}e^{l-\frac{1}{2}\theta}e^{iK\cdot r} & l>0 \end{cases}$$
$$f^B_{l,k}(\boldsymbol{r}) = \begin{cases} J_{-l-\frac{1}{2}}e^{l+\frac{1}{2}\theta}e^{iK\cdot r} & l\le 0 \\ J_{l+\frac{1}{2}}e^{l+\frac{1}{2}\theta}e^{iK\cdot r} & l>0 \end{cases} \tag{D5}$$

Note that the low-energy wavefunctions are half-integer Bessel functions naturally arising in vortex-scattering problems [41, 42]. One can now define particle and hole operators w.r.t the filled Fermi sea.

$$A^\dagger_+ \equiv a^\dagger_+, \quad A^\dagger_- \equiv a_- \quad \text{with} \quad A_\pm|M_0(\boldsymbol{R}_a)\rangle = 0 \tag{D6}$$

Similarly, we denote by B the corresponding operators using scattering states with a vison centered at position $\boldsymbol{R}_b$. Expansion of the matrix element, Eq. (D3), results in a sum of various scattering events $\sim A^\dagger B$, $AB^\dagger$, $A^\dagger B^\dagger$ and AB. For a hopping from $\boldsymbol{R}_b$ to $\boldsymbol{R}_a$, we focus on the contribution from terms of the form $A^\dagger B$. They describe processes where both initial and final states contain a single excited Majorana particle.

In contrast, the term $AB^\dagger$, for example, applied to an initial and finial states with a single excitations can be interpreted as the overlap of vison states with two excitations each. We expect that those give only subleading contributions at low T and focus instead on the $A^\dagger B$ term which is also much easier to compute.

The total transition/hopping rate for a given initial state $n_0 = \{s_0, k_0, l_0\}$ denoted by $W^{ab}(s_0,k_0,l_0) = \sum_{s,k,l}\tilde{|}w^{ab}(s0,k_0,l_0;s,k,l)|^2$ is given by

$$W^{ab}(s_0,k_0,l_0) \approx \Gamma^2\left|\langle M_0(\boldsymbol{R}_a)|M_0(\boldsymbol{R}_b)\rangle\right|^2\left(S_{s_0+}(k_0,l_0) + S_{s_0-}(k_0,l_0)\right) \tag{D7}$$

where the overlap of the ground-state wave functions $\langle M_0(\boldsymbol{R}_a)|M_0(\boldsymbol{R}_b)\rangle$ is calculated numerically for a finite size system. For a particle excitation in the inital state, $s_0 = +$, we obtain

$$S_{++}(k_0,l_0) = \frac{2\pi}{v_m}\sum_l\int\frac{dk}{2\pi}\Bigg|\sum_{l_1,l_2}\int d^2r_1 d^2r_2 w(\boldsymbol{r}_1-\boldsymbol{\delta})w(\boldsymbol{r}_2+\boldsymbol{\delta}) \int\frac{dk_1dk_2}{(2\pi)^2}\pi\sqrt{k_1k_2}\left[\eta^+_{k_1,l_1}(\boldsymbol{r}_1)\eta^{-*}_{l_2,k_2}(\boldsymbol{r}_2)\right](2\pi)^2\delta(k_0-k_1)\delta(k-k_2)\delta_{l_0,l_1}\delta_{l,l_2}\Bigg|^2\delta(k_0-k) \tag{D8}$$

where we introduce variables

$$\eta^{\pm^*}_{k,l}(\boldsymbol{r}) = e^{i\frac{\pi}{4}}f^{A^*}_{k,l}(\boldsymbol{r}) \pm e^{-i\frac{\pi}{4}}f^{B^*}_{k,l}(\boldsymbol{r}). \tag{D9}$$

To obtain S_{+-} one simply has to replace η^- by η^+ in Eq. (D8). Substituting the low energy solutions for $f_{k,l}(\boldsymbol{r})$ from Eq. (D5), the matrix elements effectively become products of half-integer Bessel functions whose arguments are shifted by the vison separation $\mathbf{2}\delta$. We can also simply replace the Wannier functions by delta functions for long-wavelength incoming Majorana excitations. Observing that the leading contribution for $k_0\delta \ll 1$ comes from the $l = 0$ state, we get

$$\begin{aligned}
S_{++}(k_0,l_0) &\approx \frac{\Omega_0^2\pi^2}{v_m}k_0^2\left|\eta^+_{k_0,l_0}(-\boldsymbol{\delta})\right|^2\left(k_0\delta + \frac{1}{k_0\delta}\right)\\
S_{+-}(k_0,l_0) &\approx \frac{\Omega_0^2\pi^2}{v_m}k_0^2\left|i\eta^+_{k_0,l_0}(-\boldsymbol{\delta})\right|^2\left(k_0\delta + \frac{1}{k_0\delta}\right)\\
S_{-+}(k_0,l_0) &\approx \frac{\Omega_0^2\pi^2}{v_m}k_0^2\left|-i\eta^{-*}_{k_0,l_0}(-\boldsymbol{\delta})\right|^2\left(k_0\delta + \frac{1}{k_0\delta}\right)\\
S_{--}(k_0,l_0) &\approx \frac{\Omega_0^2\pi^2}{v_m}k_0^2\left|\eta^{-*}_{k_0,l_0}(-\boldsymbol{\delta})\right|^2\left(k_0\delta + \frac{1}{k_0\delta}\right),
\end{aligned} \tag{D10}$$

where Ω_0 is the unit cell area. The incoherent hopping rate is obtained using the Fermi distribution n_{k_0,l_0} to sum

over the initial states.

$$W^{ab} \approx \int \frac{dk_0}{2\pi} \sum_{l_0} n_{k_0,l_0} \tilde{W}^{(1)}(k_0, l_0) = \frac{0.75\Gamma^2\Omega_0^2\pi^3}{32\beta\delta^2 v_m^2} \int du \frac{1}{1+e^u} = \frac{0.39\pi^3 a^2\Gamma^2 T}{32 v_m^2}. \quad \text{(D11)}$$

The result obtained above for a system perturbed by Γ can easily be generalized to the case where the perturbation arises from a magnetic field. In this case the perturbation can be written as

$$\Delta H_h = ih \left[b^x_{\boldsymbol{r},A} b^y_{\boldsymbol{r},A} \left(c^A_{\boldsymbol{r}} - i c^B_{\boldsymbol{r},B} \right) \left(c^A_{\boldsymbol{r}} + i c^B_{\boldsymbol{r},B} \right) \right], \quad \text{(D12)}$$

where R_a and R_b are nearest neighbour plaquettes as shown in Fig. 3b. The contribution from the c Majoranas is identical to the one in Eq. (D1) and thus we obtain the same transition rates with Γ^2 replaced by $3h^2$ where the factor 3 arises because $\delta \to \delta/\sqrt{3}$ due to the smaller hopping distance of the vison in the magnetic-field case.

Appendix E: Heisenberg interaction

In this section we argue that the single-vison hopping processes induced by the Heisenberg term at order J^2 interfere destructively. We consider a hopping across two y links as shown in Fig 7. Let us denote the hopping induced by processes depicted on the left and right side of Fig 7 by t_L and t_R. A mirror symmetry maps the processes onto each other. We now repeat the argument used in the main text to discuss the interference of hopping processes induced by Γ or h. By symmetry $t_L = \pm t_R$ and the sign will decide whether there is a destructive interference, $t_L + t_R = 0$, or a constructive interference $t_L + t_R = 2t_L$ of the two terms.

To determine the sign, we analyze a simplified question and consider the sign of

$$\tilde{t}_{L/R} = \left\langle \Phi^0(\boldsymbol{R}_1) \right| (\Delta H_J \Delta H_J)_{L/R} \left| \Phi^0(\boldsymbol{R}_2) \right\rangle, \quad \text{(E1)}$$

where we denote by $(\Delta H_J \Delta H_J)_{L/R}$ those terms which contribute to the processes on the left/right side of Fig. 7 (written below each figure). Note that $\tilde{t}_{L/R} \neq t_{L/R}$ but the two quantities are expected to have the same symmetry properties.

To map an L process to a R process we need the information on the flux configuration. The central plaquette in all diagrams in Fig. 7 does not carry any flux in the initial and final state. The plaquette operator $\hat{W} = \sigma^x_1\sigma^y_2\sigma^z_3\sigma^x_4\sigma^y_5\sigma^z_6$ has eigenvalue $+1$ (-1) in the absence (presence) of a flux [1]. Thus,

$$\left| \Phi^0(\boldsymbol{R}_2) \right\rangle = \hat{W} \left| \Phi^0(\boldsymbol{R}_2) \right\rangle = \sigma^x_1\sigma^y_2\sigma^z_3\sigma^x_4\sigma^y_5\sigma^z_6 \left| \Phi^0(\boldsymbol{R}_2) \right\rangle \quad \text{(E2)}$$

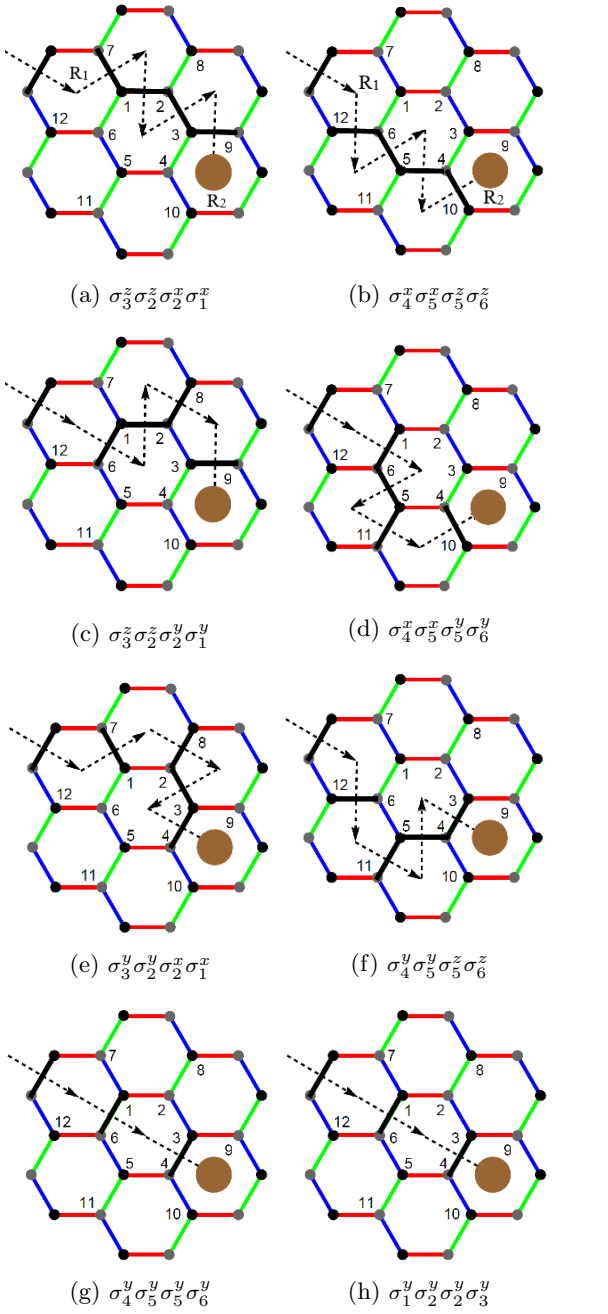

(a) $\sigma^z_3\sigma^z_2\sigma^x_2\sigma^x_1$ (b) $\sigma^x_4\sigma^x_5\sigma^z_5\sigma^z_6$

(c) $\sigma^z_3\sigma^z_2\sigma^y_2\sigma^y_1$ (d) $\sigma^x_4\sigma^x_5\sigma^y_5\sigma^y_6$

(e) $\sigma^y_3\sigma^y_2\sigma^x_2\sigma^x_1$ (f) $\sigma^y_4\sigma^y_5\sigma^z_5\sigma^z_6$

(g) $\sigma^y_4\sigma^y_5\sigma^y_5\sigma^y_6$ (h) $\sigma^y_1\sigma^y_2\sigma^y_2\sigma^y_3$

FIG. 7: Eight single-vison hopping processes ($\boldsymbol{R}_1 \to \boldsymbol{R}_2$) that pairwise interfere destructively. The dashed arrows pass though the bonds that are flipped (in black), and does not imply a multistep process.

Using this formula and the algebra of Pauli operators it is straightforward to show that

$$\left\langle \Phi^0(\boldsymbol{R}_1) \right| \sigma^x_1\sigma^x_2\sigma^z_2\sigma^z_3 \left| \Phi^0(\boldsymbol{R}_2) \right\rangle = -\left\langle \Phi^0(\boldsymbol{R}_1) \right| \sigma^z_6\sigma^z_5\sigma^x_5\sigma^x_4 \left| \Phi^0(\boldsymbol{R}_2) \right\rangle \quad \text{(E3)}$$

Therefore the processes shown in Fig. 7a and 7b contribute with opposite sign.

A straightforward extension of this argument is not

possible for all the other processes shown in Fig. 7. But a direct evaluation of $\tilde{t}_L$ and $\tilde{t}_R$ in a finite size system using the methods from App. A reveals that

$$\tilde{t}_L = -\tilde{t}_R. \tag{E4}$$

We therefore expect that $t_L = -t_R$ and processes to order J^2 thus cancel by an interference effect independent of the sign of the Kitaev coupling.

A weak Heisenberg coupling is hence expected to contribute only to order J^4 to the dispersion of single visons (as J^3 terms map a single vison to either 3 or 5 visons). Pairs of visons, however, can even hop by processes linear in J as has been shown in Ref. [32].

Appendix F: Thermal Hall conductivity of visons

In the presence of Berry curvatures, even non-interacting particles contribute to the (thermal) Hall effect. Independent of the statistics of the particles, bosonic or fermionic, the thermal hall effect at a given temperature T can be calculated from [59]

$$\kappa_{xy}(T) = -\frac{1}{T}\int_0^\infty d\epsilon\, \epsilon^2\, \sigma^v(\epsilon)\frac{\partial n}{\partial \epsilon}, \tag{F1}$$

where $n(\epsilon)$ describes the thermal occupation of the particle as function of their energy and $\sigma_{xy}(\epsilon)$ is computed from

$$\sigma_{xy}(\epsilon) = -\sum_\alpha \int \frac{d^2k}{(2\pi)^2}\boldsymbol{\Omega}_{\alpha\boldsymbol{k}}\Theta\left(\epsilon - E^v_{\alpha\boldsymbol{k}}\right) \tag{F2}$$

Note that $\sigma_{xy}(\epsilon)$ is in general *not* the electrical conductivity at temperature T but is only used to write the formula in a compact way. $\Omega_{\alpha\boldsymbol{k}}$ is the Berry curvature of a band with index α. For a single-particle Hamiltonian of the form $\boldsymbol{H}(\boldsymbol{k}) = \boldsymbol{h}(\boldsymbol{k})\cdot\boldsymbol{\sigma}$ it can be computed from $\boldsymbol{\Omega}_{\alpha\boldsymbol{k}} = \hat{\boldsymbol{h}}\cdot\left(\frac{\partial\hat{\boldsymbol{h}}}{\partial k_x}\times\frac{\partial\hat{\boldsymbol{h}}}{\partial k_y}\right)$ with the unit vectors $\hat{h}(\boldsymbol{k}) = h(\boldsymbol{k})/|h(\boldsymbol{k})|$.

To calculate the total thermal Hall effect in the presence of a magnetic field, we have to compute both the contribution from Majorana fermions and visons. Here we neglect all interaction effects which is only justified in the low-T limit when the density of visons is low.

A magnetic field h induces next-nearest neighbor hopping of Majorana fermions with amplitude t^m_{AA}. Such a hopping on the same sublattice, from A to A or B to B sublattice, breaks time-reversal symmetry and opens a gap in the Majorana spectrum. If the pure Kitaev model is perturbed only by a magnetic field, t^m_{AA} is proportional to $\frac{h^3}{K^2}$ and therefore we neglected its effect when computing the vison hopping rate linear in h. For the calculation of the thermal Hall effect, t^m_{AA} is, however, essential as it renders the Majorana bands topological. The Majorana modes $c_{\boldsymbol{k}}$ and $c_{-\boldsymbol{k}}$ can be combined to a complex Fermion, thereby reducing the size of the 1. Brillouin zone (and therefore the integral in Eq. (B3)) by a factor of 2. The thermal Hall effect is computed from using Eq. (F1) with $n(\epsilon)$ being the Fermi distribution function. At low temperature, the Majorana contribution obtains a quantized value

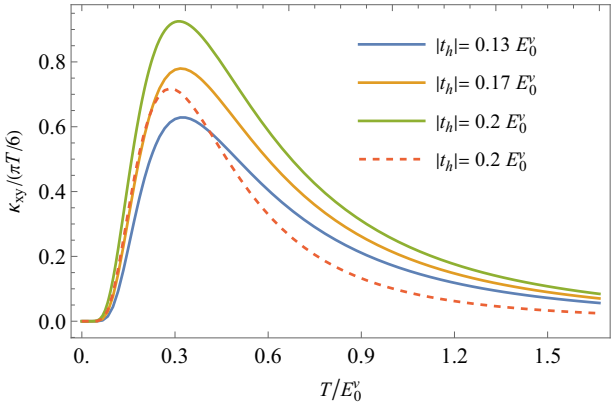

FIG. 8: Thermal hall conductivity contribution due to visons. E_v^0 is the static vison energy and t_h/E_0^v is the magnetic field induced hopping amplitude in units of $|K|$. The solid lines are computed using the Boltzmann distribution (F4), the dashed lines use a Fermi function instead, see text. The presence of a pronounced peak is a robust prediction of the theory which is, however, not valid in the high-T regime.

$$\kappa^m_{xy}(T) \approx \frac{1}{2}\frac{\pi T}{6} \quad \text{for} \quad T \ll t^m_{AA} \tag{F3}$$

In a quantum Hall system one obtains instead $\kappa^m_{xy} = n\frac{\pi T}{6}$ with integer n. The half-integer value of the prefactor $1/2$ arises because we consider Majorana particles instead of fermions. For larger T, when also the upper Majorana band gets occupied, the Majorana contribution drops. Thus it can not explain the peak in κ_{xy}/T observed experimentally [11, 13].

Exactly the same formalism can be used to calculate also the contribution to the thermal Hall effect arising from visons. Here we have, however, to take into account that each visons carries a Majorana zero mode. Thus a pair of two visons at large distance from each other carries an extra twofold degeneracy. This gives rise to an extra entropy of $\ln\sqrt{2} = \frac{1}{2}\ln 2$ per vison. In the low-density limit we can ignore any possible hybridization of these zero modes. Thus we can describe the distribution function in this limit by

$$n(E^v_{\alpha,\boldsymbol{p}}) \approx \exp\left(-\frac{E^v_{\alpha,\boldsymbol{p}} - T\ln\sqrt{2}}{T}\right) \tag{F4}$$

including the entropic correction due to the zero mode.

The vison single-particle Hamiltonian arising from the

field-induced hopping is given by

$$H^v(\boldsymbol{p}) = E_0^v \mathbb{1} + \boldsymbol{h}(\boldsymbol{p}) \cdot \boldsymbol{\sigma}$$
$$\boldsymbol{h}(\boldsymbol{p}) = 2t_h \begin{pmatrix} \sin(\boldsymbol{p}\boldsymbol{\eta}_1) \\ \cos(\boldsymbol{p}\boldsymbol{\eta}_2) \\ -\sin(\boldsymbol{p}\boldsymbol{\eta}_3) \end{pmatrix} \tag{F5}$$

with $\eta_1 = (\frac{1}{2}, \frac{\sqrt{3}}{2})$,$\eta_2 = (\frac{1}{2}, -\frac{\sqrt{3}}{2})$ and $\eta_3 = -(1, 0)$. The corresponding energies are given by $E^v_{\pm,\boldsymbol{p}} = E_0^v \pm |\boldsymbol{h}(\boldsymbol{p})|$.

In Fig. 8 we show the resulting vison contribution to the Hall conductivity, $\kappa^v_{xy}(T)$, in units of the thermal conductance quantum $\pi T/6$. At low T, the vison density and therefore also $\kappa^v_{xy}(T)$ is exponentially suppressed but one obtains a sizeable peak located at around $T \sim E_0^v/3$.

For high temperatures, when the density of visons increases, our approach is not valid any more. The statistics of the visons becomes important and vison-vison and vison-Majorana [47] interactions can no longer be ignored. There will also be skew-scattering of visons and Majorana fermions. Furthermore, the Majorana zero modes start to split when visons approach each other. To get a very rough impression when these effects set in, we replace the Boltzmann distribution, Eq. (F4), by a (entropy corrected) Fermi distribution, $n(E) = 1/(\exp\big[\beta(E - T\ln\sqrt{2})\big] + 1)$ where the Fermi function mimics the effect of the hard-core constraint which limits the number of visons per plaquette to 1. The result is shown as a dashed line in Fig. 8. We conclude that the presence of a pronounced peak is a robust prediction of the theory but that the high-temperature tail cannot be computed reliably from our approach.

Appendix G: Comparison of vison-pair and single vison gap

Vison hopping reduces the vison gap and thus is one of several mechanisms which can lead to an instability of the Kitaev spin liquid. Here it is important to consider also a second instability mechanism arising from quasi-bound states of two visons. Formally, such pairs embedded in the Majorana continuum are always unstable and have a finite lifetime. The tunneling of such vison pairs and their energy was investigated in an instructive recent study by Zhang et al. [32, 33]. Note that vison pairs carry a net flux of zero and thus their properties are very different compared to the single visons studied by us. Furthermore, we also compare the result of the two analytical studies to several numerical studies.

In Fig. 9 we show our prediction for the vison gap as function of three different perturbations (Γ, h, and J) as solid lines both for the ferromagnetic ($K < 0$) and antiferromagnetic ($K > 0$) Kitaev model. Furthermore, we show the corresponding predictions of Zhang et al. [32] for a vison pair as a dashed line. We consider only the lowest order of perturbation theory, therefore all lines are straight. The analytical treatment breaks down when the vison gap closes but one can use the results to extract trends and leading instabilities.

We first discuss the ferromagnetic Kitaev model, believed to be relevant for materials like α-$RuCl_3$ [50, 51, 53]. When perturbed by a Γ term, our results suggest that the leading instability arises from the closing of the single-vison gap, see Fig. 9a. Linear order perturbation theory obtains a closing of the gap at values roughly consistent with exact diagonalization (ED) results [27, 60] and a tensor network calculation [61]. Note, however, that a recent iDMRG study [62] predicts an increased stability of the spin liquid phase.

The situation is very different when one considers perturbations by a magnetic field h shown in Fig. 9b. Already for rather small fields, vison pairs have a lower energy compared to single visons suggesting that the condensation of vison pairs (or more complicated objects) is a prime candidate for the instability. The predicted location of the transition is again roughly consistent with ED studies.

For a perturbation by J, we do not predict any vison motion to linear order in J but there is a trivial change of the vison gap when one absorbs part of the Heisenberg coupling in the Kitaev coupling, $K \to K + J$. Here linear order perturbation theory suggests again that vison pairs become gapless first. In this case, however, the ED calculation predicts that the spin liquid is unstable for very small values of J. Therefore most likely other types of excitations or more complex bound states [32] may drive the transition.

In the antiferromagnetic case, $K > 0$, shown in the lower panel if Fig. 9 our theory makes no direct prediction as there is no vison hopping to linear order in Γ, h, and J. Compared to the ferromagnetic case, the ED results show that the system is much more stable with respect to perturbations by Γ and h, roughly consistent with the absence of single-vison tunneling linear in Γ or h in this case. The high sensitivity of the spin liquid towards tiny values of J, Fig. 9f, is, most likely, connected to the tunneling of vison pairs [32].

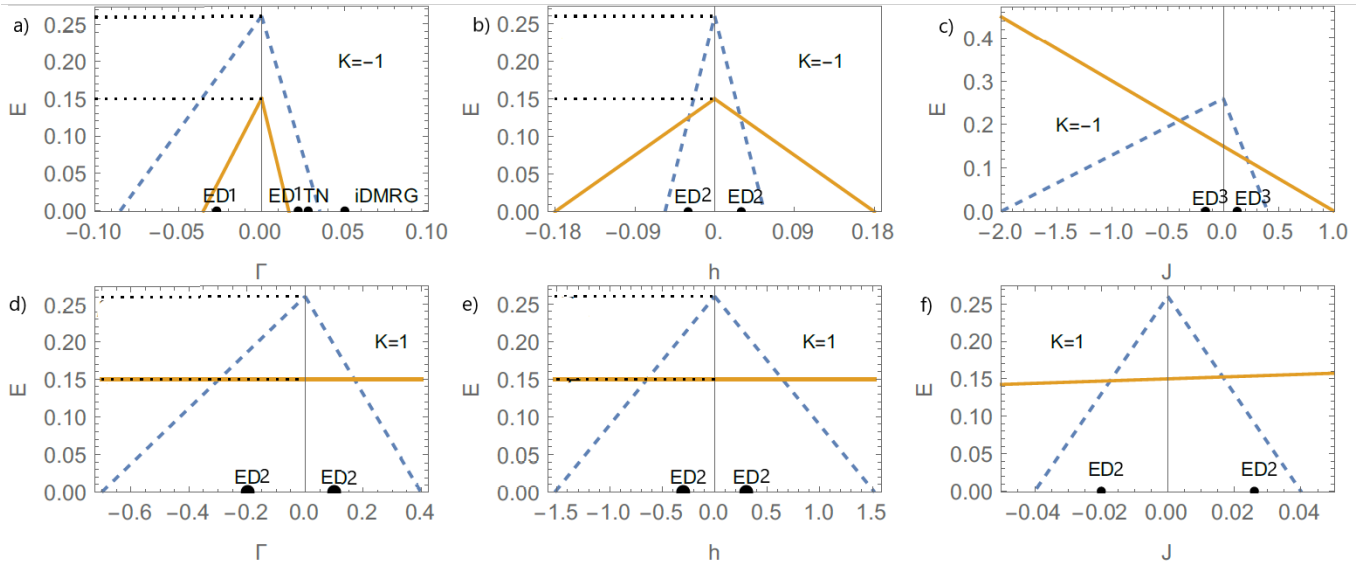

FIG. 9: Vison gap as function of Γ, h and J (solid lines in left, middle, right column) for ferromagnetic (upper panels) and antiferromagnetic (lower panels). The dashed line shows the corresponding gap of a vison pair obtained from Zhang *et al.* [32]. The thick points show numerical predictions for phase boundaries obtained from the exact diagonalization studies of Ref. [27] (ED1), Ref. [60] (ED2) and Ref. [63] (ED3), from a tensor-network based approach [61] (TN) and from an iDMRG study [62].